Mnx1 Induces Leukemia Transformation Through Altering Histone Methylation in a Model of Pediatric Acute Myeloid Leukemia with t(7;12)(q36;p13)

Ahmed Waraky[1,2], Anders Östlund[1], Tina Nilsson[2], Dieter Weichenhan[4], Pavlo Lutsik[4], Marion Bähr[4], Joschka Hey[4], Jenni Adamsson[2], Mohammad Hamdy Abdelrazak Morsy [3], Susann Li[2], Linda Fogelstrand[1,2], Christoph Plass[4] and Lars Palmqvist[1,2*]

[1]Department of Laboratory Medicine, Institute of Biomedicine, University of Gothenburg, and [2]Department of Clinical Chemistry, Sahlgrenska University Hospital, Gothenburg, Sweden.

[3]Department of laboratory medicine, division of Pathology, Karolinska institutet, Stockholm, Sweden.

[4]Division of Cancer Epigenomics, German Cancer Research Center (DKFZ), Heidelberg, Germany.

*Corresponding author

Lars Palmqvist MD, PhD

E-mail: lars.palmqvist@clinchem.gu.se

Institute of Biomedicine, University of Gothenburg

Sahlgrenska University Hospital,

SE-413 45 Gothenburg, Sweden

Phone: +46-31-3427829, Fax: +46-31-828458

ABSTRACT

Certain subtypes of acute myeloid leukemia (AML) in children have still inferior outcome. One of these AML subtypes has a translocation t(7;12)(q36;p13), always leading to high expression of MNX1 and often to *MNX1*::*ETV6* fusion expression. Here we identified the transforming event in this AML and possible ways to target them. Only MNX1 was able to induce AML in mice, and this was observed using hematopoietic stem and progenitor cells derived from fetal origin but not from adult bone marrow. The restriction in the transforming capacity to cells from fetal liver origin is in concordance with the fact that t(7;12)(q36;p13) AML is mostly restricted to infants. Ectopic expression of MNX1 led to increase of H3K4me1, H3K4me2 and H3K4me3, reduction in H3K27me3, accompanied with changes in genome-wide chromatin accessibility and genome expression, likely mediated through MNX1 interaction with the methionine cycle and different methyltransferases. MNX1 expression resulted in increased DNA damage, depletion of the Lin-/Sca1+/c-Kit+ population and skewing toward the myeloid lineage. These effects, together with leukemia development, was prevented by the S-adenosylmethionine analog Sinefungin. In conclusion, we have shown the importance of MNX1 in leukemia development in AML with t(7;12), supporting a rationale for targeting MNX1 and downstream pathways.

42 **INTRODUCTION**

43 Non-random cytogenetic aberrations are often involved in the development of acute myeloid
44 leukemia (AML) and several aberrations can serve as diagnostic markers, prognosis predictors,
45 and impact the choice of therapy (1). In AML diagnosed in children under the age of 24 months,
46 a chromosomal translocation t(7;12)(q36;p13) with poor prognosis has been reported (2). There
47 have been contradictory results on the incidence of t(7;12) but recent studies suggest the
48 frequency in children <24 months to be 5-7% (3, 4). Similarly, different results have been
49 reported regarding the prognosis where recent studies show 20%-43% 3-year event-free
50 survival but with a high relapse rate, ranging from 57-80% (3, 4). However, the understanding
51 of the mechanisms behind the leukemia transformation of t(7;12) AML remains poorly
52 understood.

53 The chromosomal break points in t(7;12) have consistently been found to be located close to
54 the Motor neuron and pancreas homeobox 1 (*MNX1)* gene on chromosome 7, and in introns 1
55 or 2 in the *ETV6* gene in chromosome 12 (5). The translocation leads to *MNX1* gene activation
56 and in most reported cases also to a *MNX1::ETV6* fusion transcript consisting of exon1 of
57 *MNX1* transcript variant 1 spliced to the remaining ETV6 exons, depending on the location of
58 the break point in ETV6 (6).

59 *MNX1,* also known as Homeobox HB9 (*HLXB9*), belongs to the homeobox domain family of
60 transcription factors, with previous studies showing the importance of *MNX1* in motor neuron
61 development (7), pancreas development (8, 9) and in hereditary sacral agenesis (10). *ETV6,* also
62 known as *TEL* belongs to the ETS-family transcription factors. *ETV6* encodes a transcriptional
63 repressor that plays a critical role in embryonic development and hematopoiesis, where it is
64 essential for normal HSC function and generation of thrombocytes by megakaryocytes (11).

Translocations involving the chromosomal region of 12p13 that result in the rearrangements of the *ETV6* gene are one of the most commonly observed chromosomal abnormalities in human leukemia with more than 30 reported translocations. These chromosomal translocations can induce leukemias through the ectopic expression of a proto-oncogene in the vicinity of a chromosomal translocation (12) or the constitutive activation of the partner protein (13). In addition, the formation of ETV6 fusion proteins can result in the modification of the original functions of the transcription factor (14), or loss of function of the fusion gene, affecting *ETV6* and the partner gene (15).

The role of the MNX1::ETV6 fusion protein in the development of AML with t(7;12) has not been established. It is also unclear whether the driver of leukemogenesis is the MNX1::ETV6 fusion protein or overexpression of MNX1. The aim of this study was to assess the transformation capacity and the molecular mechanism of the MNX1::ETV6 fusion and the ectopic expression of MNX1 *in vitro* and *in vivo* using murine transplantation models.

RESULTS

MNX1 *induces acute myeloid leukemia in hematopoietic cells of fetal origin*

To investigate the leukemogenic potential of t(7;12), we transduced primary murine (C57BL/6) hematopoietic stem and progenitor cells (HSPC) from either adult bone marrow after 5-FU stimulation (ABM-HSPC) or fetal liver cells at E14.5 (FL-HSPC) with retroviral vectors for expression of the *MNX1*::*ETV6* fusion, *MNX1*, *ETV6* or empty vector (Ctrl). Expression of *MNX1*, *ETV6* and *MNX1*::*ETV6* was confirmed in both FL-HSPC and ABM-HSPC (Supplement figure 1a-c). The transduced cells were transplanted into lethally irradiated C57BL/6 mice with rescue bone marrow. Neither *MNX1* overexpression nor *MNX1::ETV6* in ABM-HSPC or FL-HSCP were able to induce leukemia in these mice, as assessed by survival, WBC, hemoglobin, blood smears and spleen size (Supplement figure 2a-d). However, when increasing the percentage of MNX1 chimerism through sublethal radiation with no rescue BM 20% of the mice exhibited signs of malignant transformation after transplantation with FL-HSPC, including high WBCs count, severe anemia and enlarged spleen (Supplement figure 2e-f & 3a-b). To further examine the leukemogenic potential of *MNX1* overexpression and the *MNX1*::*ETV6* fusion, we repeated the experiment using immune-compromised non-irradiated NOD.Cg-Kit^{W-41J} Tyr^{+} $Prkdc^{scid}$ $Il2rg^{tm1Wjl}$/ThomJ (NBSGW) mice. Within 12-18 weeks after transplant, the *MNX1* mice showed clear signs of leukemia including pallor, weight loss, hunched posture, severe anemia, leukocytosis with a high percentage of *MNX1*-transduced cells, elevated blast cells in blood and bone marrow, enlarged spleen and liver infiltrated by leukemia (Figure 1a-c). Cells from bone marrow showed predominant expression of the myeloid marker c-Kit but not the stem cell marker SCA-1 or more differentiated myeloid markers such as MAC-1, LY6G1 and LY6C1, suggesting a poorly differentiated myeloid leukemia (Figure 1d-e). To rule out that the leukemia development in immunocompromised mice was not due to enhanced transplantation efficiency, we reduced the chimerism of *MNX1*

104 cells in NBSGW mice through the usage of lethal radiation and rescue bone marrow. These
105 mice also developed leukemia but with a slightly longer latency than mice that were sublethally
106 irradiated without rescue BM (Supplement figure 3d). Acute leukemia induction by MNX1
107 was confirmed by leukemia development after secondary transplant of BM from mice with
108 primary leukemia, both in non-irradiated mice and in sublethally irradiated mice receiving
109 rescue BM (Supplement figure 3e-f). When NBSGW mice were transplanted with ABM-HSPC
110 transduced with *MNX1*, there were no signs of leukemia six months after the transplant
111 (Supplement figure 4). Taken together, in line with t(7;12) AML occurring solely in infants,
112 leukemogenesis was achieved by MNX1 only in the immunocompromised setting with fetal
113 origin of leukemic cells.

114

115 ***MNX1 alters differentiation in favor of myeloid lineage while increasing proliferation and***
116 ***colony replating capacity of the cells***

117 In order to characterize this infant leukemia model, FL-HSPC transduced with *MNX1*::*ETV6*,
118 *MNX1*, *ETV6* or empty retroviral vector control were assessed for their immunophenotype.
119 Both *MNX1* and *MNX1*::*ETV6* altered differentiation in favor of myeloid lineage, with *MNX1*
120 showing the most prominent effects. *MNX1* increased Mac-1 and Ly6C+ cells, accompanied
121 by depletion of the Lin-/Sca1+/c-kit+ (LSK) population, while *MNX1*::*ETV6* only increased
122 Ly6C+ cells (Figure 2a-c). Ectopic expression of MNX1 reduced the progenitor MEP
123 population without affecting CMP or GMP (Supplement figure 5a). Additionally, *MNX1*
124 increased GEMM colonies with a concomitant reduction in BFU colonies and increased both
125 CFU replating and proliferation capacity (Figure 2d-f; Supplement figure 5e-f). In ABM-
126 HSPC, *MNX1* had similar effects but to a lower extent, and *MNX1*::*ETV6* fusion had no effects
127 (Supplement figure 5 b-d).

128 ***MNX1 induces DNA damage***

129 To investigate the molecular pathway through which *MNX1* is mediating its leukemogenic
130 effect, differential gene expression between *MNX1* FL-HSCP leukemic BM cells and FL-HSPC
131 transduced with empty vector (Ctrl) was assessed with RNA-sequencing (Figure 3a-d,
132 Supplement figure 6b). Gene ontology biological (GO) pathway and gene set enrichment
133 (GSEA) analyses revealed that the highest enriched pathways in *MNX1* cells involved DNA
134 damage, cell cycle, chromatin organization, methylation of histones, metabolic processes,
135 megakaryocyte, and myeloid cell differentiation pathways (Figure 3d; Supplement figure 6b).
136 Similar results were seen when using BM taken from mice transplanted with FL-HSCP with
137 empty vector as control (Supplement figure 6c-e). The effect on DNA damage was confirmed
138 through examination of γH2AX foci induction. *MNX1* and to a lower extent *MNX1::ETV6*
139 induced a higher number of γH2AX foci, indicative of higher DNA damage, in FL-HSPC as
140 well as in ABM-HSPC (Figure 4a; Supplement figure 7a). In both *MNX1* and *MNX1*::*ETV6*
141 *t*ransduced FL-HSPC, the DNA damage was accompanied with a transient G1 cell cycle
142 accumulation and fewer cells in S-phase (Figure 4b, Supplement figure 7b). No such effect was
143 observed in ABM-HSPC, where the G1 cells were replaced by a Sub-G1 peak suggestive of
144 apoptotic cells after 3-4 weeks of transduction (Supplement figure 7b). Using Annexin-V and
145 DAPI staining a 3.5-4-fold increase in apoptosis was induced by *MNX1* in ABM-HSPC, but
146 not seen in FL-HSPC (Figure 4c). Following up the consequences of such pronounced DNA
147 damage, we showed that BM from leukemia mice exhibited an increase in the amount of DNA
148 or a hyperploidy in comparison with the BM from Ctrl mice as indicated by increased DNA
149 index (Figure 4d, supplement figure 7c).

150 An interesting candidate for mediating DNA damage identified in several differentially
151 regulated pathways was the centrosomal protein 164 (*Cep164*). Increased expression of *Cep164*
152 was confirmed with qPCR in both *MNX1* transduced FL-HSPC and leukemia BM (Figure 5a).

153 Furthermore, MNX1 increased binding to the promoter of *Cep164* was detected by ChIP-qPCR
154 (Figure 5b), along with increased binding to histone modifications that can alter CEP164
155 expression namely H3K4me3 and H3K27me3 (Supplement figure 7d).

156 ***MNX1 alters histone modifications globally affecting chromatin accessibility***

157 Since MNX1 induced histone modifications H3K4me3 and H3K27me3 at the *Cep164*
158 promoter, we assessed global histone modifications. Western blotting showed that MNX1
159 altered H3K4me3, H3K27me3, and both mono- and di-methylation of the H3K4 (Figure 5c,
160 supplement figure 7e), and co-immunoprecipitation experiments (Co-IP) confirmed the
161 association of MNX1 to histone H3 (Supplement figure 7f). Antibody-guided chromatin
162 tagmentation sequencing (ACT-Seq) was then used for mapping genome-wide distribution of
163 the histone modifications (Figure 5d). H3K27me3 histone modification showed fewer
164 accessible regions in MNX1 compared to Ctrl in FL-HSPC (FDR ≤ 0.05, log2 fold change ≥
165 |1|), involving mainly distal intergenic regions followed by promoter and other intronic regions
166 (Figure 5d). The consequences of these histone modifications on chromatin accessibility were
167 investigated with ATAC-Seq. MNX1 leukemic BM cells exhibited increased number of
168 differentially accessible chromatin regions in comparison with Ctrl FL-HSPC (FDR ≤ 0.05,
169 log2 fold change ≥ |1|) (Figure 5e), mainly involving promoters, followed by distal intergenic
170 and intronic regions, very similar to the pattern seen for H3K27me3 (Figure 5d-e). Pathway
171 analysis of genes annotated to the differentially accessible regions from ATAC-Seq (FDR ≤
172 0.05, log2 fold change ≥ |1|) revealed similar pathway enrichment to the RNA-Seq, with high
173 enrichment in metabolic pathways, myeloid cell differentiation, erythrocyte differentiation,
174 cytoskeleton organization, cell cycle process and apoptotic cell process (Supplement figure 7g).
175 Further analysis through integrating ATAC-Seq data with in-silico predicted transcription
176 factor binding sites by DiffTF package, revealed 130 differentially activated sites (FDR < 0.05)
177 between MNX1 leukemic BM cells and Ctrl FL-HSPC (Table 1, Supplement figure 8a). These

178 were enriched in pathways of myeloid/erythrocyte differentiation, cellular metabolism, G1/S-
179 phase transition of cell cycle, histone methylation, DNA methylation and DNA damage
180 response (Table1, Supplement figure 8a). A significant correlation between the accessible
181 chromatin regions identified by ATAC-Seq and differentially expressed genes by RNA-Seq
182 was shown at r_S=0.47 and ($p \leq 0.01$) (Supplement figure 8b). In conclusion, MNX1 induces
183 global histone modifications that are affecting chromatin accessibility and inducing differential
184 gene regulation.

185

186 ***The effects of MNX1 on methylation are crucial for leukemogenesis***

187 In order to understand the mechanism for the MNX1-induced global histone modifications, we
188 performed mass spectrometry analysis, to study proteins in association with MNX1. MNX1
189 associated proteins were pulled down after Co-IP with anti-HA antibody. Pathway analysis
190 using STRING for protein-protein interactions for the identified proteins revealed a high
191 enrichment for methylation pathway proteins MAT2A, MAT2B and AHCY, (Figure 5f, Table
192 2), in addition to several SAM-dependent methyl transferases and their downstream targets
193 (Supplement table 1). Co-IP confirmed the association of MNX1 to MAT2A and AHCY
194 (Figure 5g, supplement figure 8c), with no effect on protein expression as shown in parallel
195 with Western blot (Supplement figure 8d). Furthermore, MNX1 overexpression increased the
196 concentration of SAH and reduced free methionine in both FL cells and leukemia BM cells
197 (Figure 5h; Supplement figure 8e-f). In support of MNX1 role in methylation pathway and in
198 altering histone methylation, MNX1 pulled down with Co-IP and incubated with recombinant
199 Histone H3 resulted in methylation of Histone H3 (Figure 5i, Supplement figure 8g). To
200 confirm the importance of this interaction for MNX1-induced leukemia, we used the natural
201 nucleoside analogue of S-adenosylmethionine Sinefungin, which acts as a SAM competitor and

202 accordingly a pan-methyltranferase inhibitor (16). Adding 5μM of Sinefungin to MNX1-
203 transduced FL-HSPC partially or completely prevented the effects of MNX1 on histone
204 modifications (Figure 6a, Supplement figure 9a), DNA damage induction (Figure 6b;
205 Supplement figure 9b), cell cycle distribution (Supplement figure 9c), myeloid differentiation
206 and LSK depletion (Figure 6c-d). Furthermore, when MNX1 FL-HSPC treated *in vitro* with
207 Sinefungin were transplanted into NBSGW mice there were no signs of leukemia development
208 (Figure 6e; Supplement figure 9d-e), despite the continuous presence of viable transplanted
209 cells in the blood (Supplement figure 9g) and maintained MNX1 expression (Supplement figure
210 9f). To confirm that Sinefungin treatment prevented leukemia transformation through inhibition
211 of methyltransferase activity in complex with MNX1 and not through the gene expression
212 downstream of methylation pathway, RNA sequencing was done before and after treatment.
213 Differentially expressed genes (FDR ≤ 0.05, log2 fold change $\geq |1.5|$) from MNX1 cells after
214 treatment (MNX+S) clustered with MNX1 (Figure 6f), and most of the differentially expressed
215 genes by MNX1 overexpression remained at similar level after treatment (Supplement figure
216 9h). Taken together, our results showed the effect of MNX1 on methylation is crucial for
217 leukemogenesis.

218

219 **DISCUSSION**

220 The t(7;12) rearrangement has only been reported in children diagnosed with AML before the
221 age of 24 months. The function of this translocation in inducing infant leukemia and the reason
222 for its absence in adult leukemia is unknown. In the current study using a murine model, we
223 showed that ectopic expression of MNX1 rather than the *MNX1*::*ETV6* fusion was able to
224 initiate and drive leukemogenesis. Our data suggest a mechanism through which MNX1 is

225 mediating the leukemogenic effect through aberrant methylation that results in histone
226 modifications and DNA damage.

227 The malignant transformation mediated by MNX1 overexpression in our mouse model matched
228 the criteria for AML (17), compatible with an AML without maturation where the development
229 of leukemia was rapidly fatal in both primary transplanted mice as well as in secondary
230 recipients. Our data showed that ectopic expression of MNX1 was only able to induce AML
231 using HSPC from fetal origin and not from adult bone marrow, primarily in
232 immunocompromised mice. This is interesting in light of the clinical observation that this AML
233 subtype is only found in very young children with peak at six months where the immune system
234 is still under development (4, 6). One possible explanation for the incapability of MNX1 ectopic
235 expression to induce leukemia from adult progenitor hematopoietic cells was further suggested
236 in our study, as the expression of MNX1 in these cells resulted in dramatic apoptotic induction,
237 which was not observed in hematopoietic progenitor cells from fetal origin. This could be due
238 to the difference in gene expression, metabolic demand, cell cycle profiles between adult and
239 fetal stem cells (18-20), the different hematopoietic lineage and progenitor population between
240 fetal and adult stem cells (21), or due to the presence of naturally occurring DNA damage in
241 the adult stem cells (22), thus making the cells more susceptible for apoptotic induction with
242 additional DNA damage induced by MNX1.

243 Studying the mechanism of MNX1 *in vitro* revealed an induction in DNA damage both in FL-
244 HSPC and ABM-HSPC, which could contribute to the observed skewed differentiation towards
245 myeloid lineage evident by the depletion of LSK and MEP population and increased Mac1+
246 and Ly6C+ population. The notion that DNA damage in stem cells might influence
247 differentiation was first demonstrated in melanocyte stem cells, where irreparable DNA
248 damage, caused by ionizing radiation triggered differentiation into mature melanocytes (23).
249 With respect to hematopoietic stem cells, DNA damage was found to induce differentiation

250 towards lymphoid lineage (24), or myeloid lineage (25). This led to the assumption that DNA
251 damage might be responsible for the skewed differentiation in the aging hematopoietic system
252 towards myelopoiesis (24-27). The consequence of this DNA damage was evident in the BM
253 from the leukemia mice with increased DNA content associated with hyperploidy. This shows
254 a resemblance to the clinical presentation where t(7;12) is associated with gain of chromosomal
255 material, typically trisomy 8 and 19 (3, 4).

256 Molecularly we found MNX1 to associate with members of the methionine cycle, including
257 MAT2A, AHCY and MAT2B, in addition to several downstream SAM-dependent methyl
258 transferases. Methionine is an essential amino acid that is converted to the universal methyl
259 donor S-adenosyl-methionine (SAM), which upon the donation of its methyl group is converted
260 to S-adenosyl-homocysteine (SAH). This reaction is catalyzed by methionine adenosyl
261 transferases (MAT). SAM is used as a cofactor in most methylation reactions and provides the
262 activated methyl group for methylation of proteins, including histones, DNA, RNA and lipids.
263 These methylation events are highly dependent on methionine metabolism, with alterations in
264 methionine showing profound effects on DNA and histone methylation (28, 29). Here, the
265 consequences effect of MNX1 on methylation and methionine cycle was observed through
266 altered histone methylation, namely H3K4me mono-, di- and trimethylation and H3K27me3,
267 which resulted in altered chromatin accessibility. The role of MNX1 in methylation/methyl-
268 transferase was shown by; a decline in the free methionine concentration; elevated SAH
269 concentration; the association of MNX1 to MAT2A and AHCY in addition to several
270 downstream SAM-dependent methyl transferase; the global alteration of histone methylation
271 H3K4me and H2K27me3; methylation of recombinant Histone H3 by MNX1 complex *invitro;*
272 pathway analysis of RNA-seq and ATAC-Seq which showed enrichment in the methylation
273 pathway, in addition to protein metabolism, a downstream pathway of methionine cycle (29,
274 30) and nucleic acid/lipid metabolism a downstream pathway of the methionine-closely linked

275 folate cycle (31, 32). This is in addition to the complete or partial prevention of MNX1
276 phenotype through the usage of the SAM/SAH analog Sinefungin (33, 34).

277 The role of homeodomain proteins in recruiting methyltransferase to regulate gene expression
278 and chromatin structure through histone modifications has been shown previously as a
279 mechanism of regulating the differentiation of myoblasts by MSX1 (35, 36). This suggests that
280 the binding and association of MNX1 with methyltranferases and members of methionine cycle,
281 and the subsequent change in chromatin structure and histone modifications, could be the
282 physiological role for MNX1 during differentiation (37, 38), and that the abnormal expression
283 of MNX1 in hematopoietic cells might act as the driver of leukemia transformation. This is
284 further supported by recent findings showing MNX1 binding to loci on chromatin to be
285 enriched for H3K4me1 and H3K4me3 during neural development (39).

286 In conclusion, our results provide the biological and clinical significance for MNX1 as an
287 epigenetic regulator in pediatric t(7;12) AML. Given that many epigenetic modifications are
288 chemically reversible, the inhibition of MNX1 ectopic expression or its downstream effects in
289 t(7;12) could provide a foundation for alternative treatment options to improve outcome.

290

291 **MATERIAL AND METHODS (Complete materials and methods in supplement)**

292 ***Plasmid constructions***

293 The *MNX1*, *ETV6* and MNX1::ETV6 fusion sequences are listed in Supplement table 2. An
294 HA-tag (36bp) is introduced at the 5' end and via a linker sequence of 24 bp attached to the
295 separate gene sequences where the first ATG is removed. These constructs were cloned into
296 the MSCV-IRES-GFP and MSCV-IRES-YFP vectors (Takara, Japan) #634401 under control
297 of the viral LTR promoter.

298 ***Generation of transduced murine bone marrow (BM) cells and transplantation assays***

299 Mice were bred and maintained at the Gothenburg university laboratory for experimental
300 biomedicine Animal Facility (Gothenburg, Sweden) in an SPF environment. Establishment and
301 characterization of BM cell lines following transduction of BM cells with *MNX1,*
302 *MNX1::ETV6, ETV6 or* empty vector Ctrl have been done as described previously (40). In brief,
303 BM cell lines were established from BM cells previously treated with 5-fluorouracil (5-FU)
304 from 8-12 weeks old (C57Bl/6) mice (Charles River Laboratories, Inc., Wilmington,
305 Massachusetts, USA) for three days for adult bone marrow (ABM) or from fetal liver at
306 embryonic days 14.5 (E14.5) and maintained in liquid culture (Dulbecco's modified Eagle's
307 medium supplemented with 18% fetal bovine serum, 10 ng/mL human interleukin [IL]-6, 6
308 ng/mL murine IL-3, and 50 ng/mL murine stem cell factor). All culture media were obtained
309 from Sigma and recombinant growth factors from Peprotech. To generate *MNX1, MNX1::ETV6*
310 *, ETV6 or* empty vector Ctrl BM cell lines, the BM cells were transduced by cocultivation on
311 irradiated (4000 cGy) E86 producers (ATCC, Manassas, VA, USA) for a period of 2 days in
312 the presence of 5 µg/mL protamine sulfate (Sigma). Cells were sorted for GFP^+ and/or YFP^+
313 expression by flow cytometry analysis (fluorescence-activated cell sorting [FACS]) FACSAria
314 (BD Biosciences) and maintained in culture for 5-7 days post transduction before

315 transplantation in mice. Lethally (8.5 Gy) or sublethally (5.5 Gy) radiated 8-12 weeks old
316 C57Bl/6 mice received the equivalent of 0.6×10^6 rescue BM cells and/or $0.8\text{-}1\times10^6$ transduced
317 cells via tail vein injection. For immunocompromised NOD.Cg-*Kit*$^{W-}$
318 ^{41J} *Tyr* $^{+}$ *Prkdc*^{scid} *Il2rg*^{tm1Wjl}/ThomJ (*NBSGW*) *mice (*The Jackson Laboratory, Bar Harbor, ME,
319 USA*)*, cells were transplanted either with no radiation, or after lethal dose of (1.6 Gy) and
320 sublethal dose of (0.9 Gy). Donor-derived engraftment and reconstitution were monitored by
321 flow cytometry analysis for GFP^+ and/or YFP^+ expression in the peripheral blood of the
322 transplants every 2 weeks. Mice were sacrificed using Isoflurane (Baxter, Deerfield, IL,
323 USA). Blood counts were analyzed on a Sysmex KX-21 Hematology Analyzer (Sysmex,
324 Norderstedt, Germany).

325 ***Immunophenotyping and flowcytometry***

326 Cells were collected 1-2 weeks after transduction. Then they were washed twice with PBS,
327 blocked with 0.1% FBS, mouse BD FC Block #553142 (BD Biosciences) in PBS for 10 mins
328 RT. Then incubated with the antibodies for 20 minutes at RT, washed and resuspended in PBS.
329 The following antibodies were purchased from BD Biosciences. Sca1-V450#560653, Cd3e-
330 V450#560801, Ter119-V450#560504, CD45R-V450#560473, Ly6G/Ly6C-V450#560454,
331 Mac1-V450#560455, Ly6G-PeCy7#560601, B220-V450#560472, CD127-V450#561205,
332 cKit-APC#553356, Sca1-PeCy7#558162, CD45-APCCy7#561037, Ter119-APC#561033,
333 CD8a-APCCy7#561967, CD4-APCCy7#561830. The following from (ThermoFisher
334 Scientific). CD115-APC#17-1152-80, CD64-APCCy7#47-0641-82.

335 For cell cycle analysis, the proportion of cells in G_1 and G_2 phases were measured by staining
336 with DAPI (BD Biosciences, #564901) as described previously (41). Briefly, cells were washed
337 with PBS, and stained DAPI solution 1:100 containing RNase A (250 μg/ml) and 0.25% Triton
338 X100 for 15 min at room temperature. The samples were processed using FACSAria (BD

339 Biosciences), and the data were analyzed with the Cell Quest software (BD Biosciences) or
340 with flowing software v 2.5.1 (Turku bioscience center, Finland).

341 Apoptosis analysis was studied using Annexin V/DAPI method (Annexin V-FLUOS staining
342 kit, Roche, Mannheim, Germany) according to the manufacturer's protocol using AnexinV-
343 APC antibody#550474 (BD Biosciences) and DAPI. Flow cytometric analysis was
344 immediately performed using FACSAria.

345 ***Statistical analysis***

346 Two-sided Student's t-test were used for comparisons between different groups in all
347 experiments. Log-rank test was used to compare survival between mice groups.

348

ACKNOWLEDGMENT

We thank Mohamad Ali and Akram Mendez for help with bioinformatic analysis. Tova Johansson and Hanna Brissman for help with animals. This work was supported by grants from the Swedish Cancer Society (20 0925 PjF), the Swedish Childhood Cancer Foundation (PR2021-0025) and Sahlgrenska University Hospital (ALFGBG-431881) to LP and Swedish Childhood Cancer Foundation (TJ2022-0017), Wilhelm och Martina Lundgrens Fond and Assar Gabrielsson Fond to AW. The German Funding Agency (DFG) with funding for Collaborative Research Center 1074, Project B11N to CP. The computations were enabled by resources in project [SNIC 2021/22-754] provided by the Swedish National Infrastructure for Computing (SNIC) at UPPMAX, partially funded by the Swedish Research Council through grant agreement no. 2018-05973.

LP, AÖ and AW designed the research study. AW, AÖ, TN, DW, PL, JH, JA, SL, MHM performed laboratory work and result analysis. AW, LF, CP and LP analyzed the combined data and wrote the paper.

Conflict of interest

The authors declare no conflict of interest associated with this paper.

Data Availability Statement

The data that support the findings of this study are available in the supplementary material of this article, from Gene Expression Omnibus (GEO) database, accession number GSE182168, GSE202137 and GSE205698 and from PRIDE/ProteomeXchange, accession number PDXD034416. Further details and other data that support the findings of this study are available from the corresponding author upon request.

Ethics Statement

372 All animal experiments have been accepted by the Jordbruksverket and the animal ethics
373 committee in Gothenburg, Dnr 5.8.18-17008/2021.

374 **REFERENCES**

375 1. Lagunas-Rangel FA, Chavez-Valencia V, Gomez-Guijosa MA, Cortes-Penagos
376 C. Acute Myeloid Leukemia-Genetic Alterations and Their Clinical Prognosis. Int J Hematol
377 Oncol Stem Cell Res. 2017;11(4):328-39.

378 2. von Bergh AR, van Drunen E, van Wering ER, van Zutven LJ, Hainmann I,
379 Lonnerholm G, et al. High incidence of t(7;12)(q36;p13) in infant AML but not in infant ALL,
380 with a dismal outcome and ectopic expression of HLXB9. Genes Chromosomes Cancer.
381 2006;45(8):731-9.

382 3. Bolouri H, Farrar JE, Triche T, Jr., Ries RE, Lim EL, Alonzo TA, et al. The
383 molecular landscape of pediatric acute myeloid leukemia reveals recurrent structural alterations
384 and age-specific mutational interactions. Nature medicine. 2018;24(1):103-12.

385 4. Espersen ADL, Noren-Nystrom U, Abrahamsson J, Ha SY, Pronk CJ,
386 Jahnukainen K, et al. Acute myeloid leukemia (AML) with t(7;12)(q36;p13) is associated with
387 infancy and trisomy 19: Data from Nordic Society for Pediatric Hematology and Oncology
388 (NOPHO-AML) and review of the literature. Genes, chromosomes & cancer. 2018;57(7):359-
389 65.

390 5. Beverloo HB, Panagopoulos I, Isaksson M, van Wering E, van Drunen E, de Klein
391 A, et al. Fusion of the homeobox gene HLXB9 and the ETV6 gene in infant acute myeloid
392 leukemias with the t(7;12)(q36;p13). Cancer Res. 2001;61(14):5374-7.

393 6. Tosi S, Mostafa Kamel Y, Owoka T, Federico C, Truong TH, Saccone S.
394 Paediatric acute myeloid leukaemia with the t(7;12)(q36;p13) rearrangement: a review of the
395 biological and clinical management aspects. Biomark Res. 2015;3:21.

396 7. Thaler J, Harrison K, Sharma K, Lettieri K, Kehrl J, Pfaff SL. Active suppression
397 of interneuron programs within developing motor neurons revealed by analysis of
398 homeodomain factor HB9. Neuron. 1999;23(4):675-87.
399 8. Li H, Arber S, Jessell TM, Edlund H. Selective agenesis of the dorsal pancreas in
400 mice lacking homeobox gene Hlxb9. Nature genetics. 1999;23(1):67-70.
401 9. Harrison KA, Thaler J, Pfaff SL, Gu H, Kehrl JH. Pancreas dorsal lobe agenesis
402 and abnormal islets of Langerhans in Hlxb9-deficient mice. Nat Genet. 1999;23(1):71-5.
403 10. Ross AJ, Ruiz-Perez V, Wang Y, Hagan DM, Scherer S, Lynch SA, et al. A
404 homeobox gene, HLXB9, is the major locus for dominantly inherited sacral agenesis. Nat
405 Genet. 1998;20(4):358-61.
406 11. Hock H, Shimamura A. ETV6 in hematopoiesis and leukemia predisposition.
407 Semin Hematol. 2017;54(2):98-104.
408 12. Rawat VP, Cusan M, Deshpande A, Hiddemann W, Quintanilla-Martinez L,
409 Humphries RK, et al. Ectopic expression of the homeobox gene Cdx2 is the transforming event
410 in a mouse model of t(12;13)(p13;q12) acute myeloid leukemia. Proc Natl Acad Sci U S A.
411 2004;101(3):817-22.
412 13. Golub TR, Barker GF, Lovett M, Gilliland DG. Fusion of PDGF receptor beta to
413 a novel ets-like gene, tel, in chronic myelomonocytic leukemia with t(5;12) chromosomal
414 translocation. Cell. 1994;77(2):307-16.
415 14. Zelent A, Greaves M, Enver T. Role of the TEL-AML1 fusion gene in the
416 molecular pathogenesis of childhood acute lymphoblastic leukaemia. Oncogene.
417 2004;23(24):4275-83.
418 15. De Braekeleer E, Douet-Guilbert N, Morel F, Le Bris MJ, Basinko A, De
419 Braekeleer M. ETV6 fusion genes in hematological malignancies: a review. Leuk Res.
420 2012;36(8):945-61.

421 16. Zhang J, Zheng YG. SAM/SAH Analogs as Versatile Tools for SAM-Dependent
422 Methyltransferases. ACS Chem Biol. 2016;11(3):583-97.
423 17. Kogan SC, Ward JM, Anver MR, Berman JJ, Brayton C, Cardiff RD, et al.
424 Bethesda proposals for classification of nonlymphoid hematopoietic neoplasms in mice. Blood.
425 2002;100(1):238-45.
426 18. Manesia JK, Xu Z, Broekaert D, Boon R, van Vliet A, Eelen G, et al. Highly
427 proliferative primitive fetal liver hematopoietic stem cells are fueled by oxidative metabolic
428 pathways. Stem Cell Res. 2015;15(3):715-21.
429 19. Bowie MB, Kent DG, Dykstra B, McKnight KD, McCaffrey L, Hoodless PA, et
430 al. Identification of a new intrinsically timed developmental checkpoint that reprograms key
431 hematopoietic stem cell properties. Proc Natl Acad Sci U S A. 2007;104(14):5878-82.
432 20. Chen C, Yu W, Tober J, Gao P, He B, Lee K, et al. Spatial Genome Re-
433 organization between Fetal and Adult Hematopoietic Stem Cells. Cell Rep. 2019;29(12):4200-
434 11 e7.
435 21. Copley MR, Eaves CJ. Developmental changes in hematopoietic stem cell
436 properties. Exp Mol Med. 2013;45:e55.
437 22. Biechonski S, Yassin M, Milyavsky M. DNA-damage response in hematopoietic
438 stem cells: an evolutionary trade-off between blood regeneration and leukemia suppression.
439 Carcinogenesis. 2017;38(4):367-77.
440 23. Inomata K, Aoto T, Binh NT, Okamoto N, Tanimura S, Wakayama T, et al.
441 Genotoxic stress abrogates renewal of melanocyte stem cells by triggering their differentiation.
442 Cell. 2009;137(6):1088-99.
443 24. Mandal PK, Rossi DJ. DNA-damage-induced differentiation in hematopoietic
444 stem cells. Cell. 2012;148(5):847-8.

445 25. Beerman I, Bhattacharya D, Zandi S, Sigvardsson M, Weissman IL, Bryder D, et
446 al. Functionally distinct hematopoietic stem cells modulate hematopoietic lineage potential
447 during aging by a mechanism of clonal expansion. Proc Natl Acad Sci U S A.
448 2010;107(12):5465-70.
449 26. Cho RH, Sieburg HB, Muller-Sieburg CE. A new mechanism for the aging of
450 hematopoietic stem cells: aging changes the clonal composition of the stem cell compartment
451 but not individual stem cells. Blood. 2008;111(12):5553-61.
452 27. Scheffold A, Baig AH, Chen Z, von Lohneysen SE, Becker F, Morita Y, et al.
453 Elevated Hedgehog activity contributes to attenuated DNA damage responses in aged
454 hematopoietic cells. Leukemia. 2020;34(4):1125-34.
455 28. Kaiser P. Methionine Dependence of Cancer. Biomolecules. 2020;10(4).
456 29. Sanderson SM, Gao X, Dai Z, Locasale JW. Methionine metabolism in health and
457 cancer: a nexus of diet and precision medicine. Nat Rev Cancer. 2019;19(11):625-37.
458 30. Parkhitko AA, Jouandin P, Mohr SE, Perrimon N. Methionine metabolism and
459 methyltransferases in the regulation of aging and lifespan extension across species. Aging Cell.
460 2019;18(6):e13034.
461 31. Zheng Y, Cantley LC. Toward a better understanding of folate metabolism in
462 health and disease. J Exp Med. 2019;216(2):253-66.
463 32. Zarou MM, Vazquez A, Vignir Helgason G. Folate metabolism: a re-emerging
464 therapeutic target in haematological cancers. Leukemia. 2021;35(6):1539-51.
465 33. Fuller RW, Nagarajan R. Inhibition of methyltransferases by some new analogs
466 of S-adenosylhomocysteine. Biochem Pharmacol. 1978;27(15):1981-3.
467 34. Couture JF, Hauk G, Thompson MJ, Blackburn GM, Trievel RC. Catalytic roles
468 for carbon-oxygen hydrogen bonding in SET domain lysine methyltransferases. J Biol Chem.
469 2006;281(28):19280-7.

470 35. Wang J, Abate-Shen C. The MSX1 homeoprotein recruits G9a methyltransferase
471 to repressed target genes in myoblast cells. PLoS One. 2012;7(5):e37647.
472 36. Wang J, Kumar RM, Biggs VJ, Lee H, Chen Y, Kagey MH, et al. The Msx1
473 Homeoprotein Recruits Polycomb to the Nuclear Periphery during Development. Dev Cell.
474 2011;21(3):575-88.
475 37. Leotta CG, Federico C, Brundo MV, Tosi S, Saccone S. HLXB9 gene expression,
476 and nuclear location during in vitro neuronal differentiation in the SK-N-BE neuroblastoma
477 cell line. PLoS One. 2014;9(8):e105481.
478 38. Dalgin G, Ward AB, Hao le T, Beattie CE, Nechiporuk A, Prince VE. Zebrafish
479 mnx1 controls cell fate choice in the developing endocrine pancreas. Development.
480 2011;138(21):4597-608.
481 39. Sun M-a, Ralls S, Wu W, Demmerle J, Jiang J, Miller C, et al. Homeobox
482 transcription factor MNX1 is crucial for restraining the expression of pan-neuronal genes in
483 motor neurons. bioRxiv. 2021:2021.08.07.455331.
484 40. Arabanian LS, Johansson P, Staffas A, Nilsson T, Rouhi A, Fogelstrand L, et al.
485 The endothelin receptor type A is a downstream target of Hoxa9 and Meis1 in acute myeloid
486 leukemia. Leuk Res. 2018;75:61-8.
487 41. Waraky A, Akopyan K, Parrow V, Stromberg T, Axelson M, Abrahmsen L, et al.
488 Picropodophyllin causes mitotic arrest and catastrophe by depolymerizing microtubules via
489 insulin-like growth factor-1 receptor-independent mechanism. Oncotarget. 2014;5(18):837992.

490

491 **FIGURE LEGENDS**

492 **Figure 1. MNX1 induces AML in immunocompromised mice.** Kaplan-Meier survival curve
493 of (NBSGW) mice transplanted with FL-HSPC after retrovirus transduction with either ectopic
494 expression of *MNX1* (green), *ETV6* (purple), *MNX1::ETV6* fusion (red) or empty vector Ctrl
495 (blue). Results from the transplanted mice (control n = 11, *MNX1*: n = 12, *ETV6* and
496 *MNX1::ETV6* n = 4) were analyzed using the log-rank test (***: significant at $P \leq 0.01$, ns:
497 non-significant) (a). Mice were euthanized at the end of the experiment and analyzed for spleen
498 weight, white blood cell number and hemoglobin concentration (b). Representative images of
499 H and E-stained formaldehyde fixed spleen and liver sections from Ctrl and MNX1 mice (e;
500 left-panels). Representative images of Giemsa-stained peripheral blood smears from Ctrl and
501 MNX1 mice (e; right-panels) (c). Representative dot plots from the flow cytometry analysis for
502 the bone marrow of the euthanized mice at the end of the experiment with the indicated
503 antibodies (d and e). Data represent mean ± SD of at least three experiments and is considered
504 significant using two-sided student t-test (**) at $p \leq 0.01$ and (*) at $p \leq 0.05$, or non-significant
505 (ns) at $p > 0.05$. FL: Fetal liver, BM: bone marrow, Ctrl: control empty vector, Fusion:
506 *MNX1::ETV6* fusion, HGB: Hemoglobin, LSK: $Lin^{-}Sca\text{-}1^{+}c\text{-}Kit^{+}$, NSG: NOD.Cg-$Kit^{W\text{-}41J}$ *Tyr*
507 $^{+}$ $Prkdc^{scid}$ $Il2rg^{tm1Wjl}$/ThomJ (NBSGW), HandE: hematoxylin and eosin.

508

509 **Figure 2. MNX1 alters differentiation and proliferation of FL-HSPC**. Representative dot
510 plots from the flow cytometry analysis of FL-HSPC transduced with ectopic expression of
511 *MNX1*, *ETV6*, *MNX1::ETV6* fusion or empty vector with the indicated antibodies (let panel, a-
512 c). Blue population represents the positive population. Quantification of the flowcytometry
513 analysis represented as percentage of population (right panel, a-c). CFU two weeks after
514 transduction of FL-HSPC (d), or weekly number of colonies with relating for five weeks (e).
515 MTT proliferation assay of transduced FL-HSPC (f). Data represent mean ± SD of at least three

516 experiments and is considered significant using two-sided student t-test (**) at $p \leq 0.01$ and (*)
517 at $p \leq 0.05$. HSPC: hematopoietic stem and progenitor cells, FL: fetal liver, Ctrl: control empty
518 vector, Fusion: *MNX1::ETV6* fusion, LSK: $Lin^{-}Sca\text{-}1^{+}c\text{-}Kit^{+}$), lin+: lineage positive, CFU:
519 colony forming unit, GM: granulocyte, macrophage, GEMM: granulocyte, erythroid,
520 macrophage, megakaryocyte, BFU: Burst-forming unit.

521

522 **Figure 3. Downstream targets of MNX1 overexpression.** LogFC heat map of downregulated
523 (blue) and upregulated (red) differentially expressed genes of leukemia BM cells with *MNX1*
524 ectopic expression in comparison with FL-HSPC with empty vector (Ctrl). Results were
525 considered at the log fold-change cutoff (logFC) of ≥ |1| and false discovery rate (FDR) of ≤
526 0.05 (a). PCA scatter plot of normalized gene expression using variance Stabilizing
527 Transformation (b). Volcano plot of differentially expressed genes (c). Gene set enrichment
528 analysis (GSEA) using the Gene ontology biological pathways (GO) gene set showing
529 normalized enrichment score for pathways with NOM p-value ≤ 0.05 (d). LogFC: Log fold
530 change, PCA: principal component analysis, FL: fetal liver, BM: Bone marrow, Ctrl: control
531 empty vector, Fusion: *MNX1::ETV6* fusion, NSG: NOD.Cg-$Kit^{W\text{-}41J}$ Tyr^{+} $Prkdc^{scid}$
532 $Il2rg^{tm1Wjl}$/ThomJ (NBSGW), PCA: principal component analysis, LogFC: Log fold change,
533 FDR: false recovery date, ChIP: chromatin immunoprecipitation.

534

535 **Figure 4. MNX1 induces DNA damage.** Immunofluorescence of FL-HSPC stained with
536 γH2AX –FITC antibody (green) and counterstained with DAPI (blue) (left panel, a).
537 Quantification of the number of γH2AX foci/cell. At least 50 cells were counted (right panel,
538 a). Representative histogram from the flow cytometry analysis of FL-HSPC and ABM-HSPC
539 after staining with DAPI for cell cycle distribution (left panel, b). Quantification of the

540 flowcytometry analysis represented as fold difference relative to control (right panel, b).
541 Representative dot plots from the flow cytometry analysis of FL-HSPC and ABM-HSPC after
542 double staining with Annexin/V and DAPI for apoptotic analysis (upper panel, c).
543 Quantification of the flowcytometry analysis represented as fold difference relative to control
544 (lower panel, c). Representative histogram from the flow cytometry analysis of BM from
545 leukemia NBSGW mice transduced with MNX1-FL cells (yellow) in comparison with
546 NBSGW mice transduced with empty vector Ctrl (red) after staining with DAPI for DNA
547 content, numbers indicated median DNA values at G1 phase and G2 phase of cell cycle. (d).
548 Quantification of DNA content in supplement figure 7c. Data represent mean ± SD of at least
549 three experiments and is considered significant using two-sided student t-test (**) at $p \leq 0.01$
550 and (*) at $p \leq 0.05$. FL: fetal liver, ABM: adult bone marrow, Ctrl: control empty vector, Fusion:
551 *MNX1::ETV6* fusion, e.A: early apoptosis, l.A: late apoptosis.

552

553 **Figure 5. MNX1 alters histone methylation.** mRNA expression of *Cep164* determined by
554 quantitative real time qPCR, normalized to *Hprt* and represented as fold difference relative to
555 control from both in vitro FL-HSPC (MNX1-FL) and BM from leukemia mice (MNX1-BM)
556 (a). Quantification of the binding of MNX1 to the promoter regions of *Cep164* in FL-HSPC
557 with either MNX1 or empty ctrl determined by ChIP-qPCR (b). Western blot analysis of
558 H3K4me1, H3K4me2, H3K4me3 and H3K27me3 in the transduced FL-HSPC. Histone 3 and
559 actin used as loading controls (c). Heatmap of differentially bound H3K27me3 from BM of
560 leukemic mice (MNX1) versus control FL-HSPC transduced with empty vector (Ctrl) as
561 determined by ACT-Seq (left panel, d). Annotation of different enriched regions for H3K27me3
562 ACT-Seq (right panel, d). Results were considered at the log fold-change cutoff (logFC) of ≥
563 |1| and false discovery rate (FDR) of ≤0.05. Heatmap of differentially accessible regions from
564 BM of leukemic mice (MNX1) versus control FL-HSPC transduced with empty vector (Ctrl)

565 as determined by ATAC-Seq (left panel, e). Annotation of different enriched regions for
566 ATAC-Seq (right panel, e). Results were considered at the log fold-change cutoff (logFC) of ≥
567 |1| and false discovery rate (FDR) of ≤0.05. Pathway enrichment analysis for the identified
568 proteins after Co-IP and mass spectrometry using STRING with reactome data set, showing
569 strength of the pathway as Log10 observed proteins/background in the respective pathway (f).
570 The binding of AHCY and MAT2A was detected by immunoprecipitation of MNX1 using HA-
571 antibody followed by western blot using AHCY and MAT2A antibodies. ETV6 with HA tag
572 was used as a negative control. Total protein input used as loading control (g). Methionine
573 concentration was determined by LC-ESI-MSMS from FL-HSPC expressing MNX1 (MNX1-
574 FL) and leukemia BM cells (MNX1-BM), normalized against total protein concentration and
575 represented as fold difference relative to control (h). Recombinant Histone H3.1and H3.3 were
576 subjected to an invitro methyltransferase reaction using MNX1 complex pulled down with HA
577 antibody from FL-HSPC transduced with MNX1(M), in comparison with FL-HSPC with empty
578 vector (C), in the presence of SAM and DTT. The reactions were terminated by boiling in SDS
579 sample buffer. Separation of samples in 12% SDS-PAGE was followed by immunoblotting
580 (IB) with mono, di and tri methyl-lysines antibody. Reblotting was made for detection of HA
581 and total Histone H3. As indicated, negative controls were obtained by omitting Histone H3, or
582 the pulled down immune complex (left panel, i). Quantification of the invitro methyltransferase
583 reaction (right panel, i). Data represent mean ± SD of at least three experiments and is
584 considered significant using two-sided student t-test (**) at $p \leq 0.01$ and (*) at $p \leq 0.05$. FL:
585 fetal liver, BM: Bone marrow, Ctrl: control empty vector, Fusion: *MNX1::ETV6* fusion, WB:
586 Western blot, ChIP: chromatin immunoprecipitation, SAM: S-Adenosyl methionine , DTT:
587 Dithiothreitol.

588

589 **Figure 6. Sinefungin rescued MNX1-induced phenotype.** Protein expression levels of
590 H3K4me3, H3k27me3, H3K4me1 and H3K4me2 in FL-HSPC with either MNX1
591 overexpression or empty vector (Ctrl) after treatment with vehicle or 5μM Sinefungin (Ctrl+S,
592 MNX1+S) as determined by Western blotting. Actin served as loading control (a).
593 Quantification of the Western blot analysis in Supplement figure 9a. Quantification of the
594 number of γH2AX foci/cell. At least 50 cells were counted. Data represented as fold difference
595 relative to control (b). Quantification of flow cytometry analysis of the cells with the indicated
596 antibodies. Data represented as fold difference relative to control (c and d). Data represent mean
597 ± SD of at least three experiments and is considered significant using two-sided student t-test
598 (**) at $p \leq 0.01$ and (*) at $p \leq 0.05$. Kaplan-Meier survival curves of (NBSGW) mice
599 transplanted with FL cells after retrovirus transduction with either ectopic expression of MNX1
600 or empty vector (Ctrl) after treatment with vehicle or 5μM Sinefungin (MNX1+S, Ctrl+S).
601 Results of MNX1 (n = 7) and Sinefungin treated MNX1 cells (MNX1+S) (n = 6) were analyzed
602 using the log-rank test (***: significant at $P \leq 0.01$) (e). Heatmap of sample distance and
603 similarity matrix for the differentially expressed genes with either ectopic expression of MNX1
604 or empty vector (Ctrl) with or without 5μM Sinefungin (Ctrl+S, MNX1+S), showing clustering
605 of cells and similarity between the samples. Results were considered at the log fold-change
606 cutoff (LogFC) ≥ |1.5| and FDR ≤ 0.05 (f). Schematic diagram for the proposed model of action
607 of MNX1 (g).

608

609 **Table 1.** In-silico predicted transcription factor binding sites by DiffTF package from ATAC-

610 Seq showing top differentially activated (FDR < 0.05) transcription factors (TFs) binding

611 between MNX1 BM from leukemia mice and FL-HSPC Ctrl cells

612

Up-regulated TFs	**weighted_mean Difference**	**pvalueAdj**	**Down regulated TFs**	**weighted_mean Difference**	**pvalueAdj**
Tal1.a	1.294844532	9.30E-79	Fosl2	-0.421333369	1.84E-24
Gata1	0.567577232	1.24E-20	Jun	-0.415408916	2.58E-23
Gata3	0.550998432	1.12E-19	Cebpe	-0.39280302	0.000108
Gata2	0.540274293	1.01E-16	Batf	-0.387629056	1.57E-17
Alx1	0.371423122	0.023026	Fosl1	-0.384618862	4.57E-21
Nf2l2	0.288226747	2.11E-17	Cebpa	-0.353311343	3.14E-06
Zeb1	0.232871599	9.60E-41	Gfi1	-0.349686909	8.73E-08
Tbx5	0.231419764	1.76E-09	Fosb	-0.339609157	5.76E-15
Mafk.s	0.22701829	3.01E-10	Sta5a	-0.339203846	2.94E-09
Nfe2	0.218904994	4.77E-11	Jund	-0.337147615	8.92E-16
Gata6	0.213067314	2.28E-11	Cebpd	-0.323368792	0.000182
Foxo3	0.202788032	0.000274	Gfi1b	-0.308823273	8.94E-12

613

614

615 **Table 2.** Identified proteins in top enriched pathways after Co-IP of proteins in complex with

616 MNX1 and mass spectrometry analysis. As determined by STRING using reactome data set

Pathway	**Matching proteins**
Association with TriC/CCT	Cct8,Cct6a,Tcp1,Cct4
Methylation	Mat2b,Ahcy,Mat2a,Trmt112
RHO GTPases activate PAKs	Ppp1cb,Myh9,Myh11,Myh10,Myh14
Citric acid cycle (TCA cycle)	Cs,Mdh2,Idh3g,Dld
Pyruvate metabolism	Pdk3,Slc16a3,Vdac1,Ldha,Dld
Actin dynamics for phagocytic	Actr2,Arpc2,Myh9,Cyfip2,Arpc3,Myo5a,Actr3
Translation initiation complex	Pabpc1,Eif3e,Rps21,Eif2s3x,Rps12,Rps28
RHO GTPase Effectors	Actr2,Mapk14,Arpc2,Ppp1cb,Myh9,Pfn1,Aurkb,S100a8,Tuba1b,Bub3,Myh11,Cyfip2,Arpc3,Myh10,Ywhaq,Myh14,Kif2a,S100a9,Actr3
Cellular Senescence	Mapk14,Asf1a,Lmnb1,Txn1,H2afz,Hist1h1b,Hist2h2be,Eed
Mitotic Anaphase	Psmd11,Aurkb,Psmd6,Lmnb1,Smc3,Psmd13,Chmp4b,Smc1a,Tuba1b,Rcc1,Bub3,Kif2a
M Phase	Psmd11,Aurkb,Psmd6,Lmnb1,Smc3,Psmd13,Chmp4b,H2afz,Smc1a,Smc4,Tuba1b,Rcc1,Bub3,Hist2h2be,Csnk2a1,Smc2,Kif2a
Metabolism of proteins	Pabpc1,Srp14,Psmd11,Rab10,Ddx5,Aurkb,Psmd6,Vdac2,Ero1l,Eif3e,Mrpl21,Smc3,Psmd13,Cct8,Srp9,Txn1,Trappc3,Cct6a,Cmas,Rab27a,Rpl22l1,Smc1a,Rpl37,Mat2b,Pdia6,Fn1,Rps21,Eif2s3x,Hist2h2ab,Rps12,Tuba1b,Ctbp1,Rpl15,Rpl36,Rpl34,Lgals1,Hist2h2be,Eef1g,Csnk2a1,Vdac1,Wdr5,Rps28,Trmt112,Tcp1,Copa,Gnb4,Ctsd,Cct4,Nop58,Tceb1
Metabolism of RNA	Pabpc1,U2af2,Psmd11,Prpf8,Snrpd3,Ddx5,Psmd6,Wdr46,Psmd13,Rpl22l1,Rpl37,Utp15,Wdr43,Rps21,Rcl1,Rps12,Rpl15,Rpl36,Rpl34,Srsf2,Nhp2l1,Snrpb,Rps28,Srsf3,Ddx6,Hnrnpd,Apobec3,Nop58

617

618

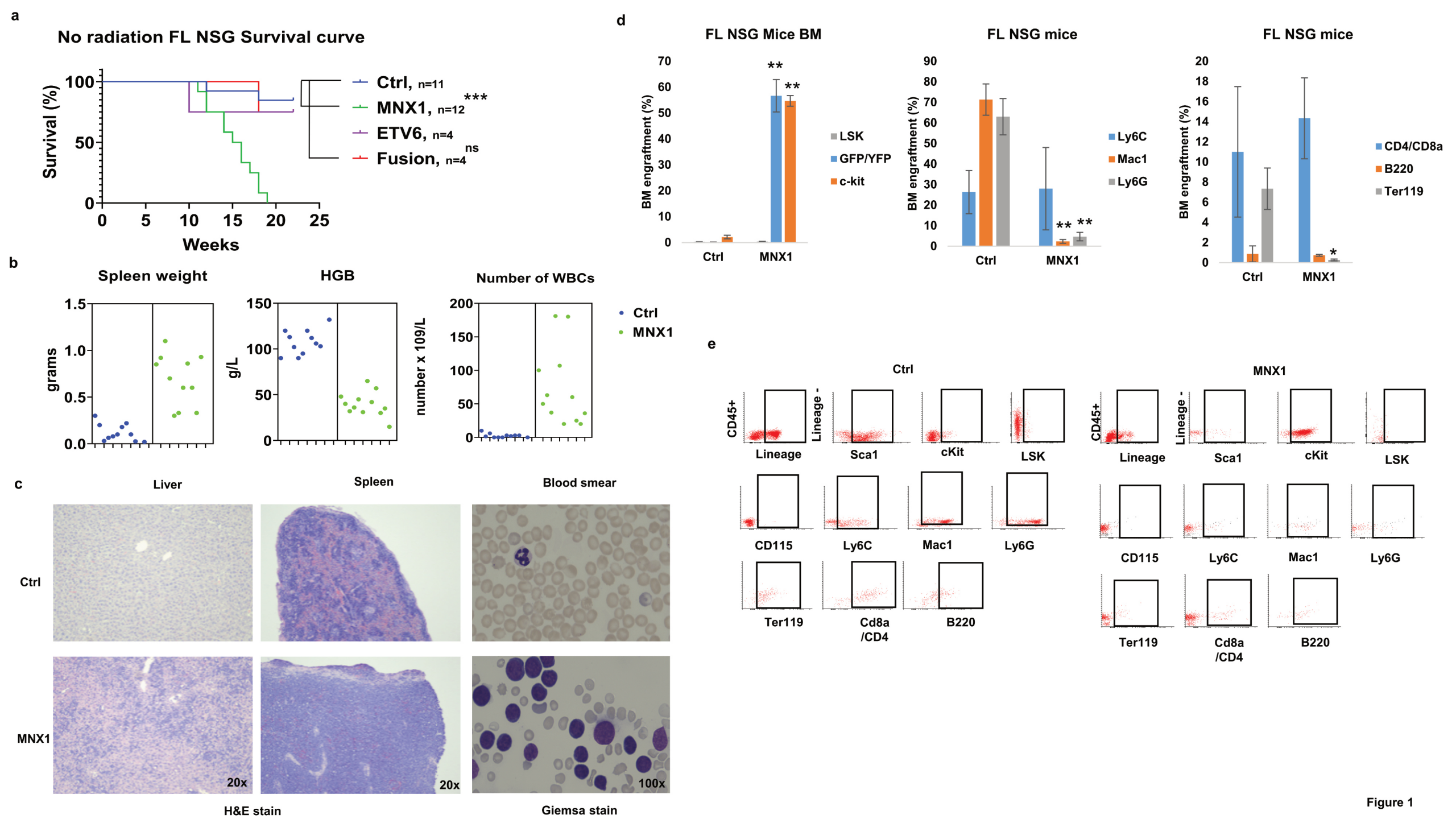
a
No radiation FL NSG Survival curve
Survival (%)
Weeks
Ctrl, n=11
MNX1, n=12
***
ETV6, n=4
Fusion, n=4
ns
b
Spleen weight
grams
HGB
g/L
Number of WBCs
number x 109/L
Ctrl
MNX1
c
Liver
Spleen
Blood smear
Ctrl
MNX1
20x
20x
100x
H&E stain
Giemsa stain
d
FL NSG Mice BM
BM engraftment (%)
LSK
GFP/YFP
c-kit
Ctrl
MNX1
FL NSG mice
Ly6C
Mac1
Ly6G
FL NSG mice
CD4/CD8a
B220
Ter119
e
Ctrl
MNX1
CD45+
Lineage -
Lineage
Sca1
cKit
LSK
CD115
Ly6C
Mac1
Ly6G
Ter119
Cd8a /CD4
B220

Figure 1

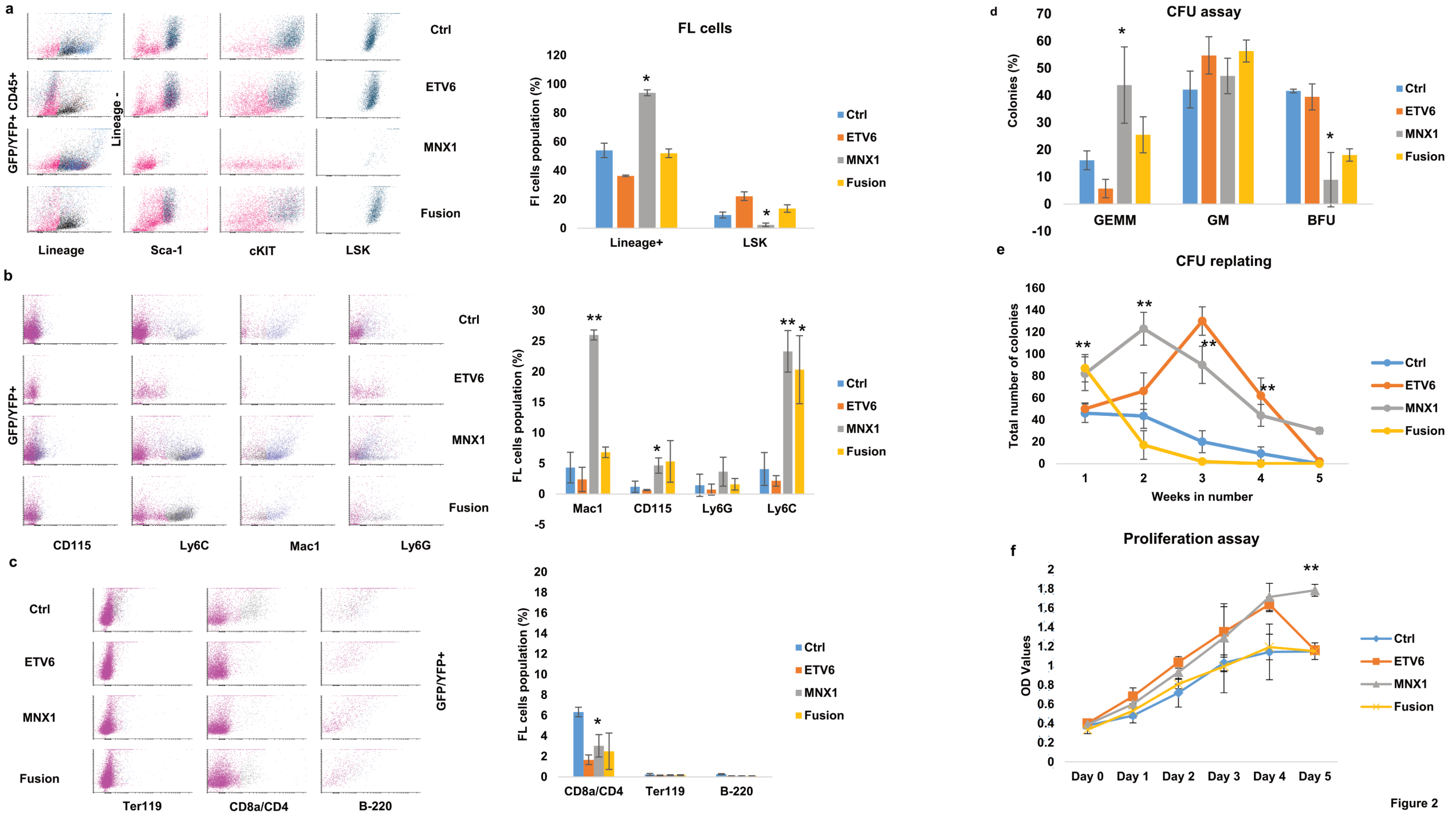
a
GFP/YFP+ CD45+
Lineage -
Ctrl
ETV6
MNX1
Fusion
Lineage
Sca-1
cKIT
LSK
FL cells
Fl cells population (%)
Lineage+
LSK
Ctrl
ETV6
MNX1
Fusion
b
GFP/YFP+
CD115
Ly6C
Mac1
Ly6G
FL cells population (%)
Mac1
CD115
Ly6G
Ly6C
c
GFP/YFP+
Ter119
CD8a/CD4
B-220
FL cells population (%)
d
CFU assay
Colonies (%)
GEMM
GM
BFU
e
CFU replating
Total number of colonies
Weeks in number
f
Proliferation assay
OD Values
Day 0
Day 1
Day 2
Day 3
Day 4
Day 5

Figure 2

a

Heatmap of RNA-seq from BM of NSG mice.
LogFC 1 and FDR ≤ 0.05

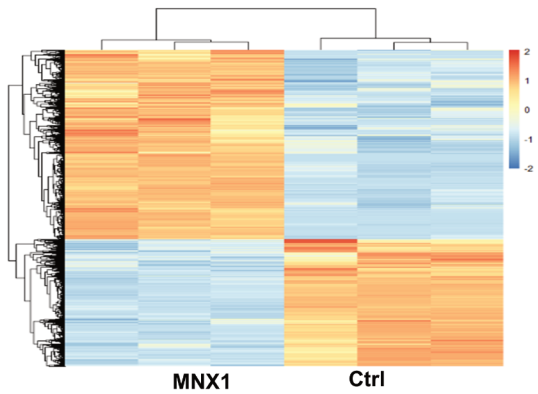

b

PCA of RNA-seq from BM of NSG mice

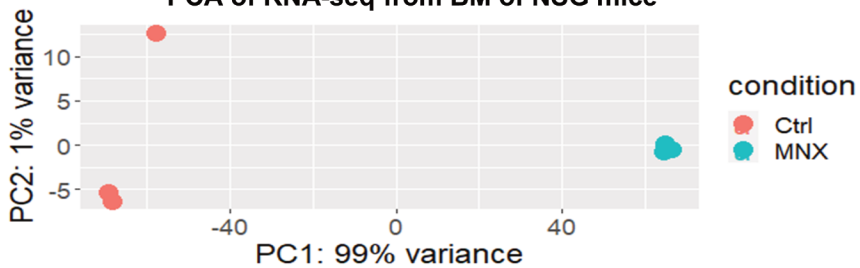

c

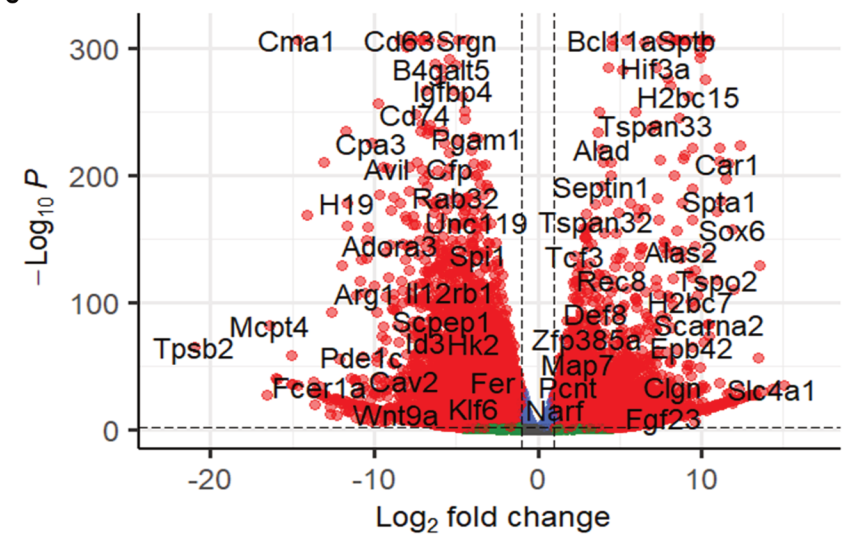

d

Gene enrichment analysis of RNA-Seq using Gene ontology gene set

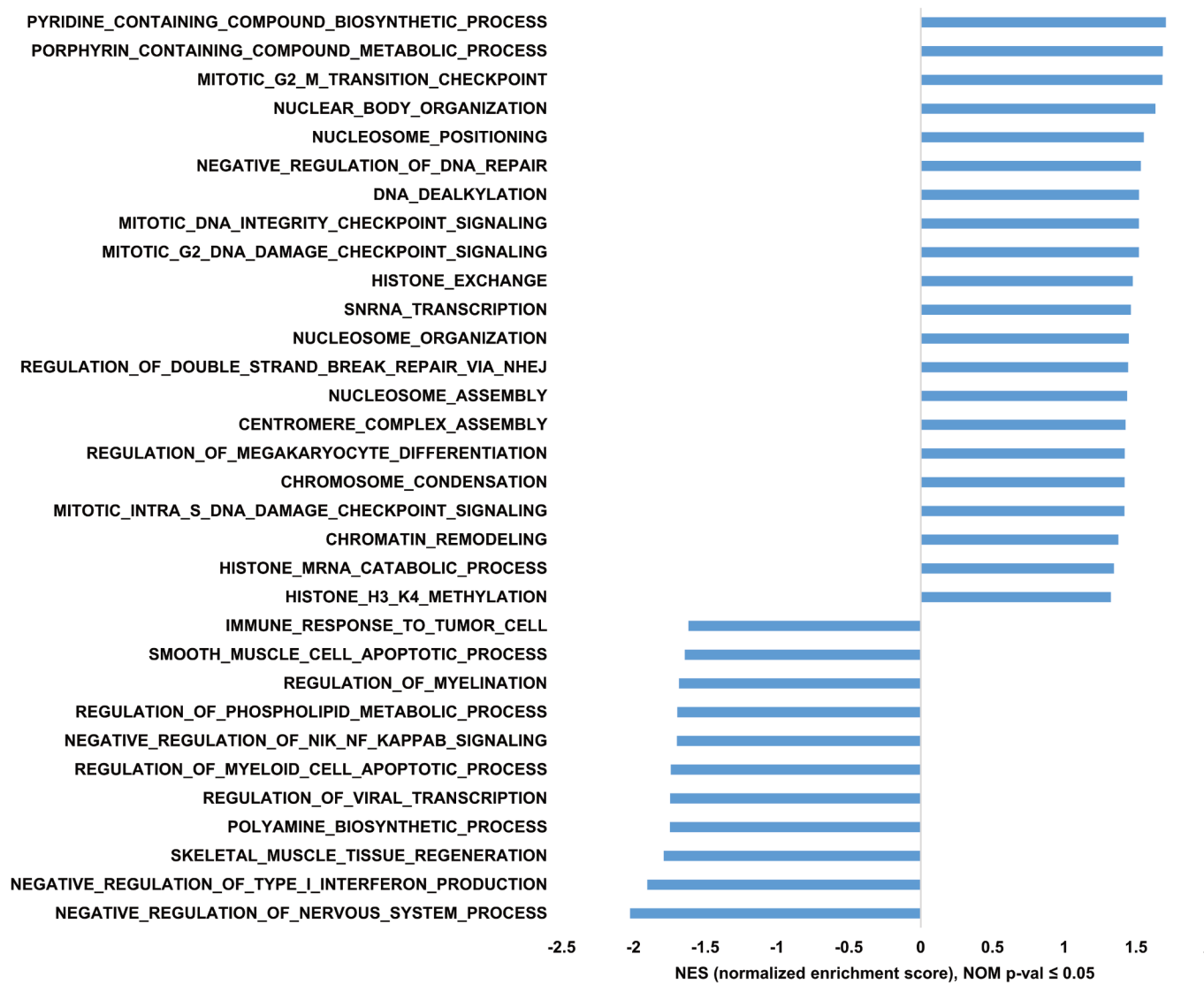

Figure 3

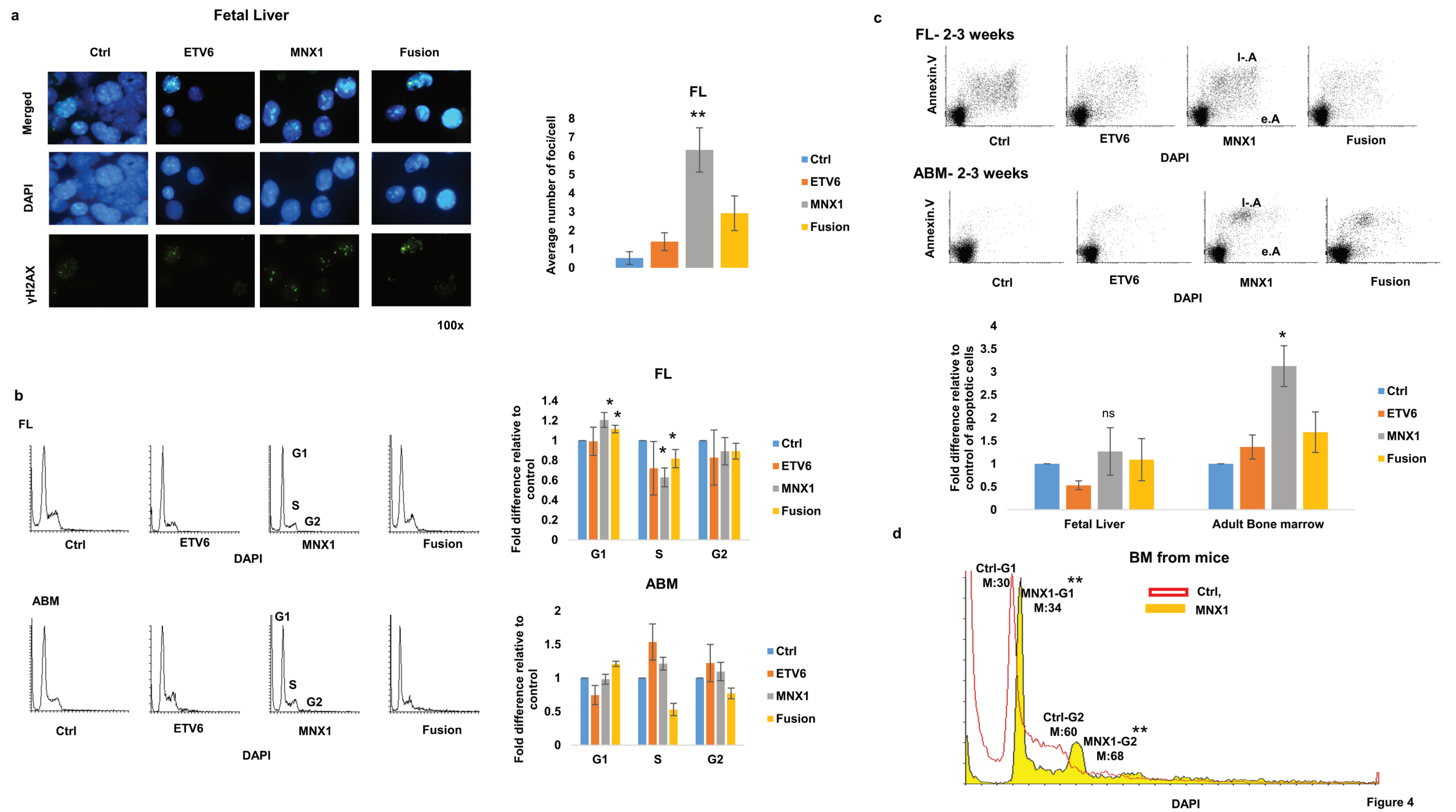
a
Fetal Liver
Ctrl
ETV6
MNX1
Fusion
Merged
DAPI
γH2AX
100x
FL
Average number of foci/cell
**
Ctrl
ETV6
MNX1
Fusion
b
FL
G1
S
G2
Ctrl
ETV6
MNX1
Fusion
DAPI
ABM
Fold difference relative to control
G1
S
G2
c
FL- 2-3 weeks
Annexin.V
I-.A
e.A
DAPI
ABM- 2-3 weeks
Fold difference relative to control of apoptotic cells
ns
Fetal Liver
Adult Bone marrow
d
BM from mice
Ctrl-G1
M:30
MNX1-G1
M:34
Ctrl,
MNX1
Ctrl-G2
M:60
MNX1-G2
M:68

Figure 4

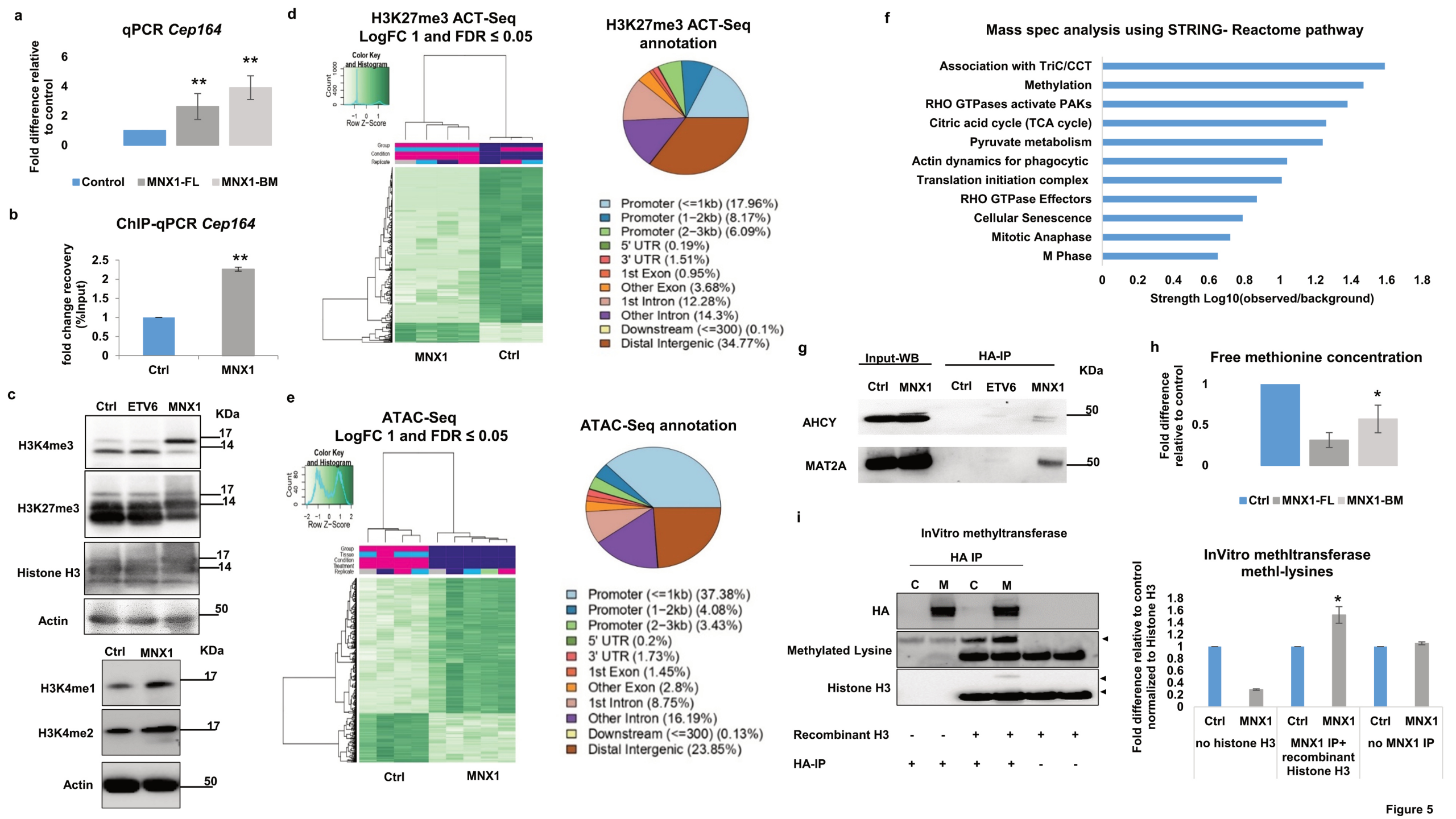
a
qPCR Cep164
Fold difference relative to control
Control
MNX1-FL
MNX1-BM
b
ChIP-qPCR Cep164
fold change recovery (%Input)
Ctrl
MNX1
c
Ctrl
ETV6
MNX1
KDa
H3K4me3
H3K27me3
Histone H3
Actin
H3K4me1
H3K4me2
d
H3K27me3 ACT-Seq
LogFC 1 and FDR ≤ 0.05
Color Key and Histogram
Row Z-Score
H3K27me3 ACT-Seq annotation
Promoter (<=1kb) (17.96%)
Promoter (1−2kb) (8.17%)
Promoter (2−3kb) (6.09%)
5' UTR (0.19%)
3' UTR (1.51%)
1st Exon (0.95%)
Other Exon (3.68%)
1st Intron (12.28%)
Other Intron (14.3%)
Downstream (<=300) (0.1%)
Distal Intergenic (34.77%)
e
ATAC-Seq
LogFC 1 and FDR ≤ 0.05
ATAC-Seq annotation
Promoter (<=1kb) (37.38%)
Promoter (1−2kb) (4.08%)
Promoter (2−3kb) (3.43%)
5' UTR (0.2%)
3' UTR (1.73%)
1st Exon (1.45%)
Other Exon (2.8%)
1st Intron (8.75%)
Other Intron (16.19%)
Downstream (<=300) (0.13%)
Distal Intergenic (23.85%)
f
Mass spec analysis using STRING- Reactome pathway
Association with TriC/CCT
Methylation
RHO GTPases activate PAKs
Citric acid cycle (TCA cycle)
Pyruvate metabolism
Actin dynamics for phagocytic
Translation initiation complex
RHO GTPase Effectors
Cellular Senescence
Mitotic Anaphase
M Phase
Strength Log10(observed/background)
g
Input-WB
HA-IP
AHCY
MAT2A
h
Free methionine concentration
Fold difference relative to control
i
InVitro methyltransferase
HA IP
HA
Methylated Lysine
Histone H3
Recombinant H3
HA-IP
InVitro methltransferase methl-lysines
Fold difference relative to control normalized to Histone H3
no histone H3
MNX1 IP+ recombinant Histone H3
no MNX1 IP

Figure 5

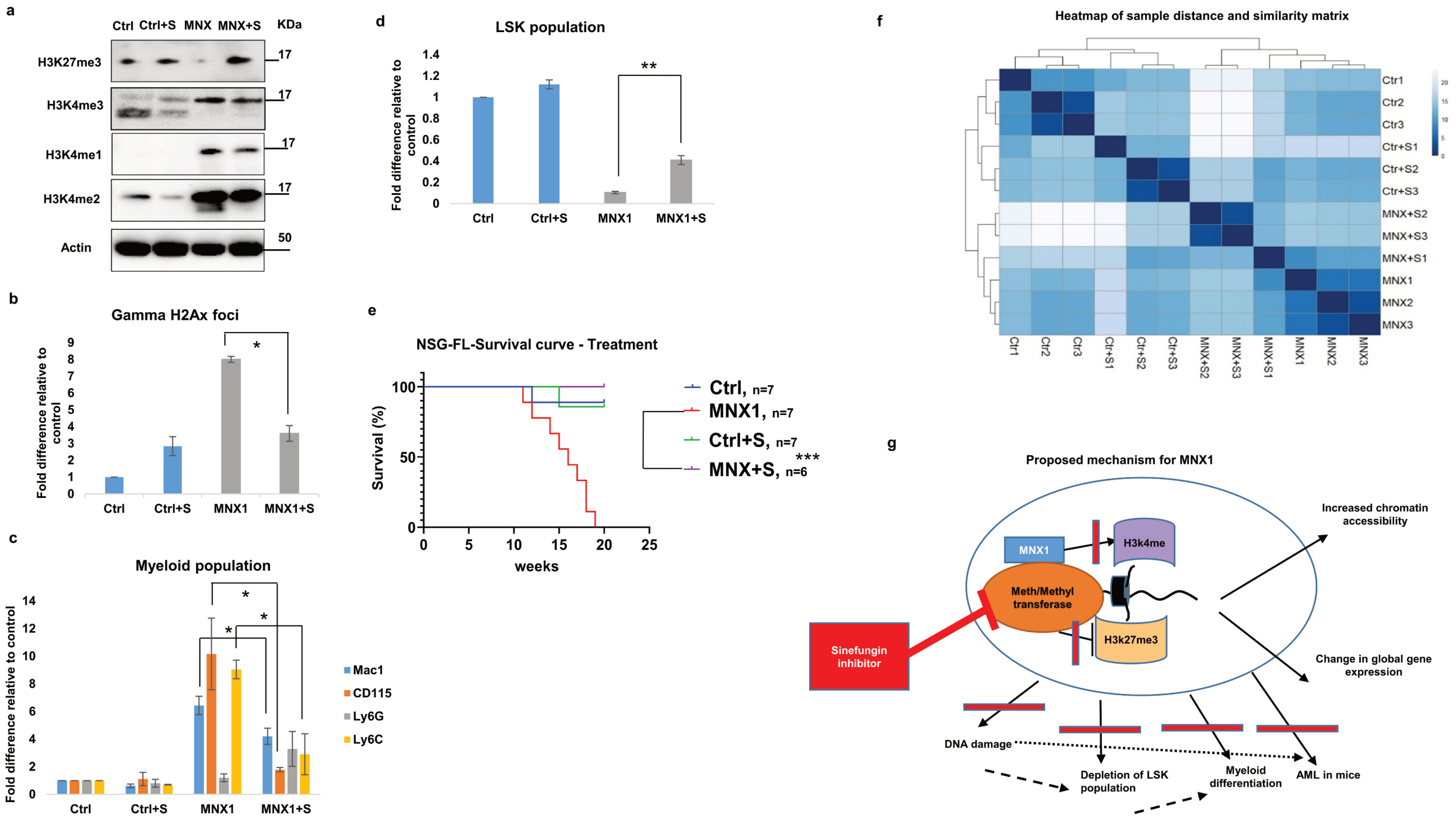
a
Ctrl Ctrl+S MNX MNX+S KDa
H3K27me3
H3K4me3
H3K4me1
H3K4me2
Actin
17
17
17
17
50
b
Gamma H2Ax foci
Fold difference relative to control
Ctrl
Ctrl+S
MNX1
MNX1+S
c
Myeloid population
Fold difference relative to control
Mac1
CD115
Ly6G
Ly6C
d
LSK population
Fold difference relative to control
Ctrl
Ctrl+S
MNX1
MNX1+S
e
NSG-FL-Survival curve - Treatment
Survival (%)
weeks
Ctrl, n=7
MNX1, n=7
Ctrl+S, n=7
MNX+S, n=6
f
Heatmap of sample distance and similarity matrix
Ctr1
Ctr2
Ctr3
Ctr+S1
Ctr+S2
Ctr+S3
MNX+S2
MNX+S3
MNX+S1
MNX1
MNX2
MNX3
g
Proposed mechanism for MNX1
MNX1
H3k4me
Meth/Methyl transferase
H3k27me3
Sinefungin inhibitor
Increased chromatin accessibility
Change in global gene expression
DNA damage
Depletion of LSK population
Myeloid differentiation
AML in mice

Figure 6